Eur. Phys. J. D (2014) 68: 40
DOI: 10.1140/epjd/e2013-40395-7

THE EUROPEAN PHYSICAL JOURNAL D

Regular Article

Effect of current on multiple pinches of Xe plasma in capillary discharge

Qiang Xu[1], Yongpeng Zhao[1,a], Yao Xie[2], Yang Liu[1], Qi Li[1], and Qi Wang[1]

[1] National Key Laboratory of Tunable Laser Technology, Harbin Institute of Technology, Harbin 150080, P.R. China
[2] State Key Laboratory of Applied Optics, Changchun Institute of Optics, Fine Mechanics and Physics, Chinese Academy of Sciences, Changchun 130033, P.R. China

Received 7 July 2013 / Received in final form 2 August 2013
Published online 4 March 2014 – © EDP Sciences, Società Italiana di Fisica, Springer-Verlag 2014

Abstract. The effect of the current on the pinching process of Xe plasma columns pumped by capillary discharge has been studied theoretically and experimentally. An extreme ultraviolet emission monitor (E-Mon, 13.5 nm in 2% bandwidth) was applied to record the temporal evolution of the 13.5 nm (2% bandwidth) emission. According to real current waveforms, the pinching processes were simulated with the snow-plow model. Both the experimental and the simulation results showed that intensity of the 13.5 nm emission reached the maximum when the plasma was pinched to the minimum radius. The E-Mon signals and the simulations indicated that under different amplitudes of the currents the plasma could be pinched more times and faster with higher discharge current.

1 Introduction

Extreme ultraviolet (EUV) lithography technology, which uses the 13.5 nm emission in a 2% bandwidth will be used for high volume semiconductor manufacturing (HVM) under at 16 nm node or even below, has been investigated comprehensively [1,2]. Here the choice of wavelength of 13.5 nm is mainly due to the peak reflectivity at this wavelength for molybdenum-silicon (Mo/Si) multilayer mirrors [3].

In 1998, Klosner and Silfvast reported the first experimental results that demonstrated the capability of the Xe capillary discharge technology as the EUV source [4]. Since then, many papers have been published on the prospects of utilizing it as the EUV lithography tool [5,6]. Due to the higher convention efficiency (CE) of the 13.5 nm emission [7–9], Sn based EUV source has replaced Xe as one of the main sources to achieve HVM. Meanwhile, the medium and low power Xe based EUV sources for applications such as metrology and test of the optical elements, the resist, the EUV-mask and so on are studied as well [10–12]. The typical sources are the Bruker AIXUV EUV-lamp [10] and the Energetiq EQ-10 [13], which use the HCT pinch technology and the Electrodeless Z-pinch technology respectively to achieve high power 13.5 nm (2% bandwidth) emission. The gas discharge principle provides long time stability and minimum maintenance [10] by comparison with the laser produced plasma EUV source or the Sn based EUV source. The capillary discharge EUV source reported in this paper, using the Lorentz force to pinch the plasma and achieve 13.5 nm emission, is essentially the same as the aforementioned sources. Hence, the study on pinch processes in capillary is useful for other types of gas discharged EUV sources.

Until now, a great many key physical and technical issues for the capillary discharge plasma have been investigated. The temporal evolution of the 13.5 nm (2% bandwidth) emission is still one of the important issues. Mohanty et al. found that the plasma inside the capillary channel had two minimum radii by a pinhole with higher discharge voltage [14,15], which is different from other results [4,16]. However, they did not give the theoretical explanation. In Teramoto's experimental results, there are more than two peaks for the temporal evolution of the 13.5 nm emission [17]. According to their hypothesis, the peaks may be generated from the uniform implosion or the multiple implosions of the plasma. However, they did not give a quantitative explanation. In this paper, an E-Mon (EUV Monitor) is used to record the temporal evolutions of the 13.5 nm (2% bandwidth) emission with different discharge currents, whose structure is similar to the EUV inband energy monitor (Bruker Advanced Supercon GmbH, 00M-EM-001) or the reference [18]. And the effect of the SiN filter in this paper is similar to the Zr filter in the EUV energy monitor. The experimental results show that there is one signal peak of the E-Mon signals at a discharge current of 15 kA. However, as the magnitude of discharge current increases, more peaks tend to show up and simultaneously the 13.5 nm emission is boosted [19]. In order to have a better understanding on the physical

[a] e-mail: zhaoyp3@yahoo.com.cn

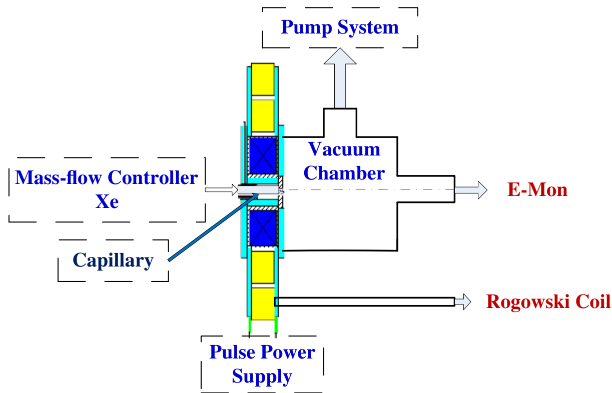

Fig. 1. Cross sectional view of the capillary discharge system.

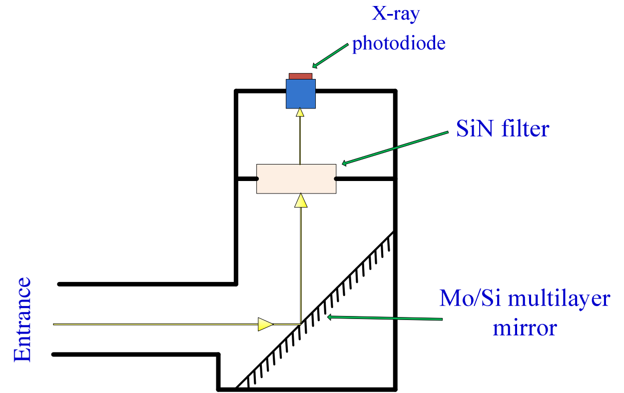

Fig. 2. Cross sectional view of the E-Mon detector.

correlation between the 13.5 nm emission and the pinching process, a snow-plow model was used to simulate the dynamic characteristics of the Xe plasma by comparing with the experimental results.

2 Experimental setup

Figure 1 shows the cross sectional view of the capillary discharge system used for generating the EUV radiation in the experiment. It consists of the pulse power supply system, the discharge system and the detection system. The pulse power supply system includes the main-pulse power supply and the pre-pulse power supply. The capillary is pre-discharged by a current pulse of about 10 A to first produce a uniform pre-ionized Xe gas. The delay time of the main-pulse power supply to the pre-pulse power supply is 5 μs.

The main-pulse voltage ranged from 15 kV to 30 kV, and the current ranged from 15 kA to 40 kA. The current was measured by a Rogowski coil and recorded by a digital oscilloscope (Tektronix, DPO3054). The response time of the coil is 2 ns. Xe gas was used as a EUV emitter and was continuously flowing through the capillary. An alumina capillary with a 7 mm inner diameter and 12 mm length used. The discharge device was mounted onto a vacuum pumping assembly that maintained a uniform pressure of Xe gas within the capillary. The pressure in the capillary was controlled by a mass-flow controller to adjust the gas flow rate from 0.4 cm^3 min^{-1} to 2.0 cm^3 min^{-1}, with approximately 0.1 Pa of residual air pressure in the capillary prior to the admission of Xe.

Figure 2 shows the cross sectional view of the E-Mon detector. It consists of a Mo/Si multilayer mirror, a SiN filter and a fast-response X-ray photodiode (AXUV20HS1BNC, 10%–90% rise-time 2 ns). The E-Mon detector is mounted at the central axis of the capillary to measure the temporal evolution of the 13.5 nm (2% bandwidth) emission.

The size for the entrance of the E-Mon detector is much smaller than that for the Mo/Si multilayer mirror. Therefore the signals that pass through the SiN filter should be those that reflected by the Mo/Si multilayer mirror. The signal detected by the X-ray photodiode should be only the 13.5 nm emission in 2% bandwidth. Moreover, caused by the coax, the X-ray photodiode and the Rogowski coil, the delay time between the E-Mon system and the current detection system is 16 ns. In this paper, all the results have been corrected for the delay time of the current and the 13.5 nm emission.

3 Results and analysis

The current waveforms (curve A) and the E-Mon signals (curve B) are shown in Figure 3 at two main currents. The flow rate of the Xe gas is 0.7 cm^3 min^{-1}. Both of the two different main current pulses have 10%–90% rise-time of 97 ns. However, the emission signal sustains for a longer time with higher current. In addition, there are three peaks of the EUV signal for the current of 28 kA, which differs that of 15 kA which shows only from one peak.

Figure 3 also shows that the first peak of the E-Mon signal appears at 98 ns with the current of 15 kA, and the three peaks for the current of 28 kA at 92 ns, 127 ns and 158 ns. These observations appear to indicate that the higher current leads to the earlier appearance of the peak of the EUV emission and more peaks of the E-Mon signals. The values of the first peak at the currents of 15 kA and 28 kA are 2.5 V and 3.2 V respectively. The integrated E-Mon signal indicates the 13.5 nm (2% bandwidth) emission pulse energy. The ratio of the two E-Mon signals for the two currents shown was calculated be 7: 16. Therefore, the 13.5 nm intensity increases with higher discharge current.

In order to understand the results, we simulate the pinching process with a snow-plow model. In this model, the main equation is as follows [20]:

$$\frac{d}{dt}\left[\pi\rho_0\left(a^2-r^2\right)\frac{dr}{dt}\right] = -\frac{\mu_0 I^2}{4\pi r} + 2\pi r P \qquad (1)$$

where ρ_0 is the initial gas density in the capillary, a and r are the inner radius of the capillary and the radius of the plasma sheet, I is the main current and P is the pressure in the plasma column. In order to use the fourth-order step Runge-Kutta method to calculate the equation

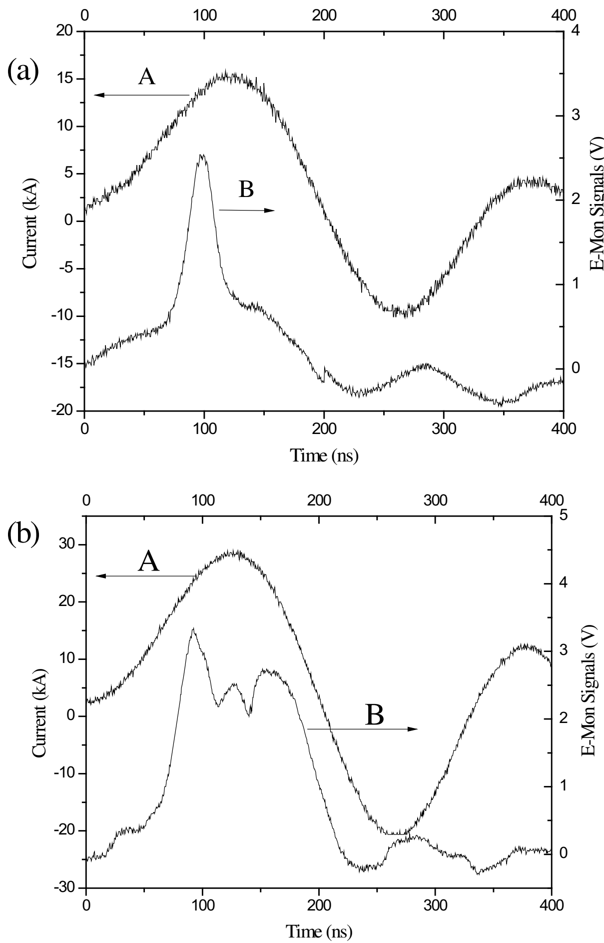

Fig. 3. The waveforms of the main discharge current (A) and the E-Mon signal (B).

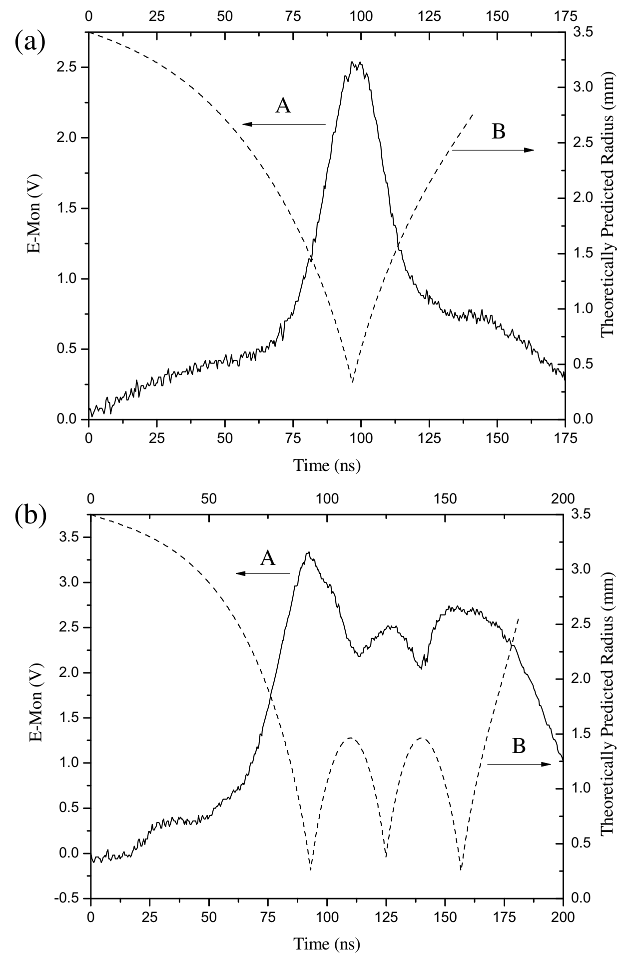

Fig. 4. The waveforms of the E-Mon output signals (A) and the theoretically predicted evolution of the plasma radius (B). The peak values of the main discharge currents are 15 kA (a) and 28 kA (b).

numerically, equation (1) is rewritten as two differential equations [21,22]:

$$\frac{dr_1}{dt} = -\frac{\mu_0 I^2}{4\pi r} + 2\pi r P \tag{2}$$

$$\frac{dr}{dt} = \frac{r_1}{\pi\rho_0(a^2 - r^2)}. \tag{3}$$

According to snow-plow model [23], the pressure P of the plasma in equation (1) includes the inner kinetic pressure p_{in} and outer kinetic pressure p_{out}. According to P. Vrba's opinion, "the outer kinetic pressure is usually neglected $p_{out} = 0$, as no ablation from the capillary wall is taken into account", and the inner kinetic pressure is expressed as $p_{in} = p_0(V_0/V)^{5/3} = p_0(r_1/a)^{10/3}$. Here p_0 is the initial gas pressure.

Under general conditions, I is a function of time and is fitted to an analytic function. However, Figure 2 shows that the current waveforms cannot be fitted to an analytic function accurately. Consequently, the measured digital data of the current waveform was used to calculate the equations directly.

Figure 4 shows the simulation results for the two main currents in Figure 3. In Figure 4, the solid lines correspond to the E-Mon signals, and the dashed lines correspond to the evolution of plasma radius. To compare the time of the 13.5 nm with the pinching time, the E-Mon signals in Figures 3a and 3b are correspondingly redrawn in Figures 4a and 4b. The simulation results show that there is only one pinch for the current of 15 kA, compared to the multiple pinches obtained with the current of 28 kA. The 13.5 nm emission reaches a maximum value when the plasma is pinched to the minimum radius. Moreover, the first pinching time decreases with the increase of current value as well.

For the current of 15 kA, the plasma is pinched to the minimum radius when the current attains its maximum value according to Figure 3a. At this moment, the kinetic pressure is balanced by the magnetic pressure. Then the kinetic pressure becomes higher than the magnetic pressure and the plasma radius will consequently increase. Due to the decrease of the current with time, the magnetic pressure should be no longer higher than the kinetic pressure. As a result, there is only one pinch for the current of 15 kA. On the other hand, there are three peaks of the E-Mon signals with the current of 28 kA. When the plasma

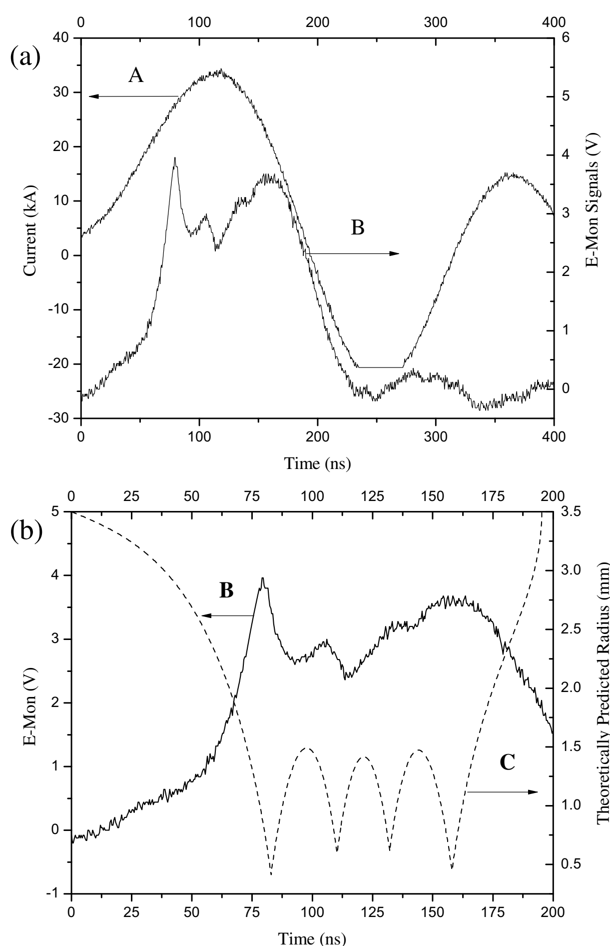

Fig. 5. The waveforms of the main current (A), the E-Mon output signal (B) and the theoretically predicted evolution of the plasma radius (C). The peak value of the main current is 34 kA.

is pinched to the minimum radius for the first time, there is a balance between the kinetic pressure and the magnetic pressure, which is similar to the condition at 15 kA. Due to the decrease of the kinetic pressure and the increase of the magnetic, the latter of which is generated by the increase of the current as shown in Figure 3b, the plasma will be pinched again. The second or third implosion occurs if the current is still high enough to compress the plasma. The simulation results as depicted in Figure 5b show that the radius of the plasma reaches its minimum value more than once also.

In order to further confirm this deduction, the main current was increased to 34 kA. The flow of Xe is the same as Figures 3 and 4. The waveform of the main current, the E-Mon output signal and the simulation result for the evolution of the plasma radius are showed in Figure 5.

As shown in Figure 5, at 34 kA, there are four peaks occurring during both the rise-time and the fall-time of the main current of E-Mon signals which again in a well agreement with the simulation result indicates that the plasma is pinched to the minimum radius four times correspondingly. These results demonstrate further that higher main current makes the plasma pinch more often.

In addition, the first peak of the E-Mon signal appears at 80 ns, 92 ns and 98ns respectively according to Figures 4 and 5. Correspondingly, the simulation results show that the time for the plasma to be firstly pinched to the minimum radius are 83 ns, 93 ns and 97 ns respectively. Thus, one can concludes that higher current leads to faster pinching under the same gas pressure.

4 Conclusion

The Xe gas 13.5 nm (2% bandwidth) emission pumped by capillary discharge was studied theoretically and experimentally. An E-Mon was used to record the temporal evolution of the 13.5 nm (2% bandwidth) emission. The experimental results showed that the 13.5 nm emission existed almost during the first peak of the current. Changing the discharge current, we simulated the evolution of the plasma radius and observed the temporal evolutions of the 13.5 nm (2% bandwidth) emission. By comparing experimental results with the simulation results, we can find that when the plasma was pinched to the minimum radius, the 13.5 nm emission reached the maximum value. The radius of the plasma in the simulations and the evolution of the 13.5 nm emission indicated that the Xe plasma was pinched faster and more times by higher current. From the results we deduced that there were multiple pinches for high enough discharge current. These results should be useful to better understand the pinching process of the plasma for capillary discharge system or the EUV source.

This work is supported by the Project supported by the Key Program of the National Natural Science Foundation of China (No. 60838005) and the Project supported by the National Science and Technology Major Project of the Ministry of Science and Technology of China (2008ZX02501).

References

1. K. Bergmann, O. Rosier, W. Neff, R. Lebert, Appl. Opt. **39**, 3833 (2000)
2. J.V. Hermans, D. Laidler, C. Pigneret, A.V. Dijk, O. Voznyi, M. Dusa, E. Hendrickxa, *Conference on Extreme Ultraviolet (EUV) Lithography II* (2011), Vol. 7969, p. 79691M
3. C. Zaczek, S. Müllender, H. Enkisch, F. Bijkerk, *Conference on Advances in Optical Thin Films III* (2008), Vol. 7101, p. 71010X
4. M.A. Klosner, W.T. Silfvast, Opt. Lett. **23**, 1609 (1998)
5. K. Nowakowska-Langier, L. Jakubowski, E. Baronova, K. Czaus, M. Rabinski, M.J. Jakubowski, Eur. Phys. J. D **54**, 377 (2009)
6. K. Bergmann, G. Schriever, O. Rosier, M. Muller, W. Neff, R. Lebert, Appl. Opt. **38**, 5413 (1999)
7. K. Nishihara, A. Sunahara, A. Sasaki, M. Nunami, H. Tanuma, S. Fujioka, Y. Shimada, K. Fujima, H. Furukawa, T. Kato, Phys. Plasmas **15**, 056708 (2008)
8. J. White, P. Hayden, P. Dunne, A. Cummings, N. Murphy, P. Sheridan, G. O'Sullivan, J. Appl. Phys. **98**, 113301 (2005)

9. B.A. Hansson, L. Rymell, M. Berglund, O. Hemberg, E. Janin, J. Thoresen, S. Mosesson, J. Wallin, H.M. Hertz, *Conference on Emerging Lithographic Technologies VI* (2002), Vol. 4688, p. 102
10. R. Lebert, B. Jagle, C. Wies, U. Stamm, J. Kleinschmidt, K. Gaebel, G. Schriever, J. Pankert, K. Bergmann, W. Neff, *Conference on 21st European Mask and Lithography Conference* (2005), Vol. 5835, p. 230
11. S.F. Horne, M.M. Besen, D.K. Smith, P.A. Blackborow, R. D'Agostino, *Conference on Emerging Lithographic Technologies X* (2006), Vol. 6151, p. 61510P
12. M.J. Partlow, M.M. Besen, P.A. Blackborow, R. Collins, D. Gustafson, S.F. Horne, D.K. Smith, J. Micro/Nanolith. MEMS MOEMS **11**, 021105 (2012)
13. S.F. Horne, M.J. Partlow, D.S. Gustafson, M.M. Besen, D.K. Smith, P.A. Blackborow, *Conference on Extreme Ultraviolet (EUV) Lithography III* (2012), Vol. 8322, p. 83222M
14. S.R. Mohanty, E. Robert, R. Dussart, R. Viladrosa, J.M. Pouvesle, C. Fleurier, C. Cachoncinlle, Microelectron. Eng. **65**, 47 (2003)
15. J. Pouvesle, E. Robert, T. Gonthiez, R. Viladrosa, J. Pons, O. Sarroukh, M. Idrissi, B. Metay, S. Mohanty, C. Fleurier, Plasma Sources Sci. Technol. **12**, S43 (2003)
16. N.R. Fornaciari, H. Bender, D. Buchenauer, M.P. Kanouff, S. Karim, G.D. Kubiak, C.D. Moen, G.M. Shimkaveg, W.T. Silfvast, K.D. Stewart, *Conference on Emerging Lithographic Technologies V* (2001), Vol. 4343, p. 226
17. Y. Teramoto, H. Sato, K. Bessho, K. Miyauchi, M. Ikeuchi, K. Okubo, M. Yoshioka, K. Toyoda, *Conference on Emerging Lithographic Technologies VII* (2003), Vol. 5037, p. 767
18. A. Hidenori, K. Sunao, N. Takao, S. Takashi, I. Hideki, in *Powder Modulator Symposium, 2006. Conference Record of the 2006 Twenty-Seventh International, Arlington, VA, USA* (IEEE, 2006), pp. 356–359
19. T. Boboc, R. Bischoff, H. Langhoff, J. Phys. D **34**, 2512 (2001)
20. Y. Hayashi, N. Sakamoto, Y.P. Zhao, Y.L. Cheng, P. Chalise, M. Watanabe, A. Okino, K. Horioka, E. Hotta, Plasma Sources Sci. Technol. **13**, 675 (2004)
21. Y. Zhao, Y. Cheng, B. Luan, Y. Wu, Q. Wang, J. Phys. D **39**, 342 (2006)
22. Y. Zhao, Q. Wang, Y. Xie, Y. Cheng, B. Luan, J. Plasma Phys. **74**, 839 (2008)
23. P. Vrba, M. Vrbová, Contrib. Plasma Phys. **40**, 581 (2000)